Earth and Planetary Science Letters 408 (2014) 66–78

Contents lists available at ScienceDirect

Earth and Planetary Science Letters

www.elsevier.com/locate/epsl

Imaging the Antarctic mantle using adaptively parameterized P-wave tomography: Evidence for heterogeneous structure beneath West Antarctica

Samantha E. Hansen [a], Jordan H. Graw [a], Lindsey M. Kenyon [a], Andrew A. Nyblade [b], Douglas A. Wiens [c], Richard C. Aster [d], Audrey D. Huerta [e], Sridhar Anandakrishnan [b], Terry Wilson [f]

[a] Geological Sciences Department, The University of Alabama, Tuscaloosa, AL 35487, United States
[b] Geosciences Department, Pennsylvania State University, University Park, PA 16802, United States
[c] Department of Earth and Planetary Sciences, Washington University in St. Louis, MO 63130, United States
[d] Geosciences Department, Colorado State University, Fort Collins, CO 80523, United States
[e] Department of Geological Sciences, Central Washington University, Ellensburg, WA 98926, United States
[f] Earth Sciences Department, The Ohio State University, Columbus, OH 43210, United States

ARTICLE INFO

Article history:
Received 21 May 2014
Received in revised form 23 September 2014
Accepted 26 September 2014
Available online xxxx
Editor: P. Shearer

Keywords:
Antarctica
seismic tomography
mantle structure
geodynamics

ABSTRACT

Previously developed continental-scale surface wave models for Antarctica provide only broad interpretations of the mantle structure, and the best resolved features in recent regional-scale seismic models are restricted above ~300–400 km depth. We have developed the first continental-scale P-wave velocity model beneath Antarctica using an adaptively parameterized tomography approach that includes data from many new seismic networks. Our model shows considerable, previously unrecognized mantle heterogeneity, especially beneath West Antarctica. A pronounced slow velocity anomaly extends between Ross Island and Victoria Land, further grid south than previous studies indicate. However, at least for mantle depths ≥~200 km, this anomaly does not extend grid north along the Transantarctic Mountains (TAMs) and beneath the West Antarctic Rift System. The boundary between these slow velocities and fast velocities underlying East Antarctica is ~100–150 km beneath the front of the TAMs, consistent with flexural uplift models. The lateral extent of the low velocity anomaly is best explained by focused, rift-related decompression melting. In West Antarctica, Marie Byrd Land is underlain by a deep (~800 km) low velocity anomaly. Synthetic tests illustrate that the low velocities also extend laterally below the transition zone, consistent with a mantle plume ponded below the 660 km discontinuity. The slow anomalies beneath Ross Island and Marie Byrd Land are separate features, highlighting the heterogeneous upper mantle of West Antarctica.

1. Introduction

Present continental-scale seismic images of Antarctica generally show East Antarctica underlain by fast seismic velocities, thought to be associated with a stable Precambrian craton, with West Antarctica underlain by slow velocities, interpreted as the signature of continental rifting (*e.g.*, Ritzwoller et al., 2001; Sieminski et al., 2003; Morelli and Danesi, 2004; Suppl. Fig. 1). While these models illustrate the dichotomous nature of the mantle beneath Antarctica, their spatial resolution (~600–1000 km) is insufficient to delineate velocity variations within either geographic domain, allowing for only broad interpretations of the lithospheric and sub-lithospheric mantle structure. Regional seismic investigations (*e.g.* Watson et al., 2006; Lawrence et al., 2006a; Heeszel et al., 2013; Lloyd et al., 2013a) have highlighted more variable structure beneath Antarctica, but the limited aperture of the networks used in these studies often makes the lateral and vertical extent of velocity anomalies difficult to determine. To further characterize the geologic processes shaping the Antarctic continent, higher resolution, broad-scale images of the seismic structure across Antarctica are required.

Using a large quantity of recently available seismic data from several high-quality broadband deployments in Antarctica (*e.g.* Anthony et al., submitted for publication) and an adaptively parameterized tomography approach (Kárason, 2002; Li et al., 2008;

E-mail address: shansen@geo.ua.edu (S.E. Hansen).

http://dx.doi.org/10.1016/j.epsl.2014.09.043
0012-821X/

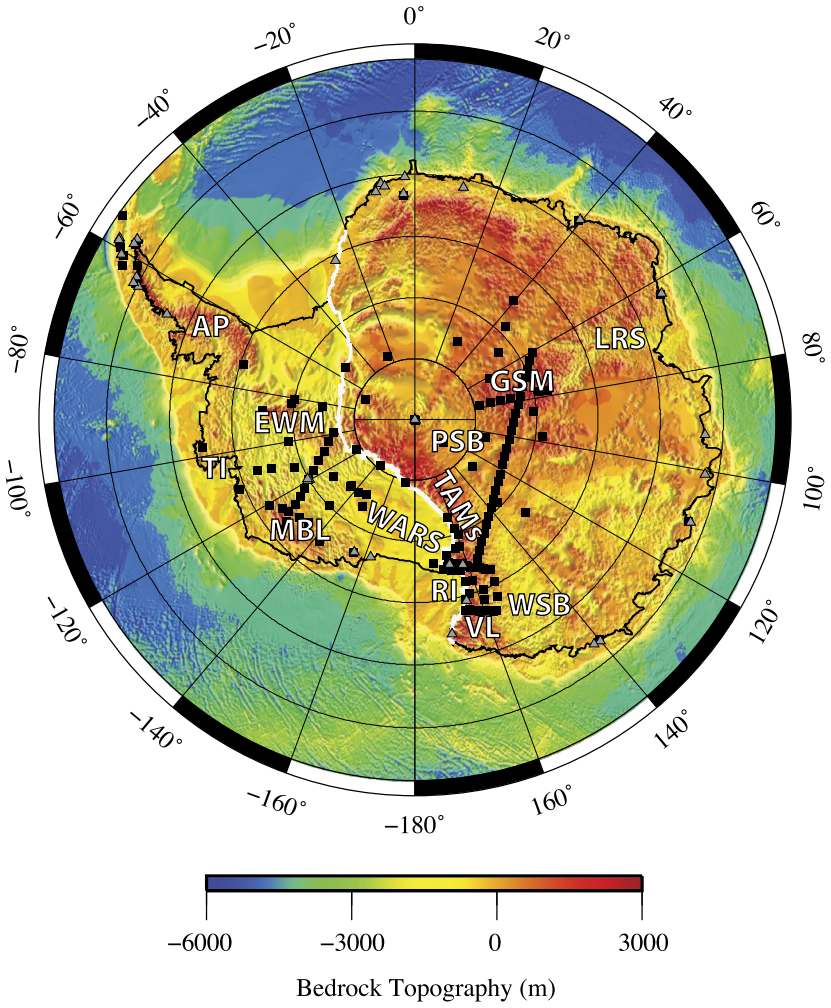

Fig. 1. Subglacial bedrock topography across Antarctica from BEDMAP2 (Fretwell et al., 2013). The white line denotes the Transantarctic Mountains-defined boundary between East and West Antarctica. Grey triangles and black squares mark the EHB and Antarctic regional network stations, respectively, used in this study. GSM: Gamburtsev Subglacial Mountains, LRS: Lambert Rift System, PSB: Polar Subglacial Basin, TAMs: Transantarctic Mountains, WSB: Wilkes Subglacial Basin, VL: Victoria Land, RI: Ross Island, WARS: West Antarctic Rift System, MBL: Marie Byrd Land, EWM: Ellsworth–Whitmore Mountains, TI: Thurston Island, AP: Antarctic Peninsula. Modified from O'Donnell and Nyblade (2014).

Hansen et al., 2012), we have developed the first continental-scale model of P-wave speed variations in the Antarctic mantle. This approach, which combines multiple, regional travel-time datasets in the context of a global model, yields a tomographic image with finer-scale resolution of mantle structure beneath Antarctica compared to previously developed continental-scale models. Additionally, the tomographic image obtained has higher resolution at greater mantle depths than reported for regional-scale tomographic models. Improved tomographic results, particularly at mid-mantle depths, are important for evaluating competing geologic models. Our model reveals considerable, previously unrecognized heterogeneity in the Antarctic mantle, especially beneath West Antarctica. Specifically, distinct and separate low velocity anomalies are imaged beneath Ross Island (RI) and Marie Byrd Land (MBL). The lateral and depth extent of these anomalies provides new insight into the geodynamic processes associated with rifting and hotspot tectonism in West Antarctica.

2. Geologic background and previous studies

Antarctica is broadly divided into two main tectonic domains: East Antarctica and West Antarctica, which are separated by the Transantarctic Mountains (TAMs; Fig. 1). Widespread Archean and Proterozoic outcrops along the East Antarctic coast (Tingey, 1991) and similar Proterozoic rocks in the TAMs (Goodge et al., 2001) have led many to propose that the East Antarctic interior is a vast Precambrian craton (Tingey, 1991; Dalziel, 1992; Hoffman, 1991; Moores, 1991; Rogers et al., 1995). Other studies have suggested a more complicated tectonic history for East Antarctica, including multiple Proterozoic, Paleozoic, and even Cenozoic orogenic events (Zhao et al., 1995; Liu et al., 2002; Fitzsimons, 2000, 2003; Ferraccioli et al., 2011).

West Antarctica comprises an amalgamation of several tectonic blocks, including MBL, Thurston Island (TI), the Ellsworth–Whitmore Mountains (EWM), and the Antarctic Peninsula (AP; Fig. 1). Lithospheric stretching between these blocks and within the Ross Embayment led to the initial formation of the West Antarctic Rift System (WARS) at ~100 Ma (Fig. 1; Stock and Molnar, 1987; Bradshaw, 1989; Lawver et al., 1991). Another phase of rifting in the Cenozoic (Fitzgerald and Baldwin, 1997) was accompanied by volcanism along parts of the TAMs, in MBL, and probably within the WARS interior (Behrendt et al., 1997; Siddoway, 2008). Some models for the WARS suggest that all major extension and heating of the upper mantle occurred during the late Cretaceous and that any Cenozoic activity is limited to isolated locations, such as the Terror Rift near RI (Fig. 1; Wannamaker et al., 1996; Karner et al., 2005). Other models suggest that moderate levels of extension have continued to occur to the present and that the

upper mantle remains thermally perturbed (Cande et al., 2000; Granot et al., 2010).

Unlike many other mountain ranges of similar size, the TAMs show no evidence for a compressional origin. Apatite fission track dating indicates that the main phase of TAMs uplift began ~55 Ma, leading to as much as 7–8 km of uplift in some locations (Fitzgerald, 1992, 1994; Sutherland et al., 2011), although the rate of uplift is still somewhat controversial (*e.g.*, Barrett et al., 1989; Clapperton and Sugden, 1990; Behrendt and Cooper, 1991). The lack of compressional structures in the TAMs has led to much debate regarding their origin, and a variety of uplifted models have been proposed (*e.g.*, Fitzgerald et al., 1986; Stern and ten Brink, 1989; Bott and Stern, 1992; Chéry et al., 1992; van der Beek et al., 1994; ten Brink et al., 1997; Studinger et al., 2004; Karner et al., 2005; Lawrence et al., 2006b).

Crustal thickness estimates across East Antarctica average ~35–45 km (*e.g.* Groushinsky and Sazhina, 1982; von Frese et al., 1999; Ritzwoller et al., 2001; Reading, 2006; Block et al., 2009; Ferraccioli et al., 2011). More detailed regional seismic studies show thick crust (55–58 km) beneath the Gamburtsev Subglacial Mountains (GSM) in central East Antarctica, with thinner crust (40–45 km) in the surrounding areas (Hansen et al., 2010; Heeszel et al., 2013; O'Donnell and Nyblade, 2014) and evidence for crustal thinning (~34 km) near South Pole and the Polar Subglacial Basin (PSB; Fig. 1). Crustal thickness estimates in the WARS range from ~17 km in parts of the Ross Embayment to ~37 km beneath the EWM (*e.g.* ten Brink et al., 1993; Clarke et al., 1997; Yoo, 1998; Winberry and Anandakrishnan, 2004; O'Donnell and Nyblade, 2014; Chaput et al., 2014). The large variation in crustal thickness suggests large spatial variability in the degree of extension across the WARS (Studinger et al., 2002). Beneath the TAMs, the crust appears to thicken from about 25–30 km near the Ross Sea to 40–45 km some 100–150 km inland (ten Brink et al., 1993; Lawrence et al., 2006b; Hansen et al., 2009; Finotello et al., 2011; Chaput et al., 2014).

Previous continental-scale seismic images of Antarctica, which have been generated using surface wave analyses and fairly sparse station coverage, show seismically fast upper mantle beneath East Antarctica, indicating thick lithosphere, with seismically slow upper mantle beneath the WARS. The boundary between these two regions roughly coincides with the TAMs (Suppl. Fig. 1; *e.g.* Roult and Rouland, 1994; Ritzwoller et al., 2001; Sieminski et al., 2003; Morelli and Danesi, 2004). Within either tectonic domain, the velocities are fairly homogeneous. For instance, Ritzwoller et al. (2001) and Morelli and Danesi (2004) display highly smoothed seismic velocities models across East and West Antarctica, with only about a 1% velocity variation in either tectonic domain. The depth extent of these models is ~300–400 km. Sieminski et al. (2003) used higher mode Rayleigh waves to image deeper mantle structure (to ~600 km depth) but again, the velocities across both East and West Antarctica are fairly uniform (Suppl. Fig. 1).

Regional-scale seismic investigations show more heterogeneity in the mantle structure beneath Antarctica. For example, Heeszel et al. (2013) and Lloyd et al. (2013a) imaged slower mantle velocities beneath the PSB and the Lambert Rift System (Fig. 1) in East Antarctica (albeit still faster relative to global averages), suggesting thinner lithosphere under these areas. Beneath MBL, slow velocities extending to at least ~300–400 km depth have been observed, in contrast with faster mantle velocities beneath the EWM (Heeszel, 2011; Lloyd et al., 2013b). Lawrence et al. (2006a) and Watson et al. (2006) imaged an upper mantle low velocity anomaly beneath RI, extending 50–100 km beneath the TAMs. However, the limited aperture of these regional studies makes the lateral and depth extent of these various velocity anomalies difficult to constrain, thereby leading to questions about the associated geodynamic processes.

3. Data and methodology

Our new P-wave tomography model for Antarctica has been developed using an adaptive parameterization method (Kárason, 2002; Li et al., 2008), described by Hansen et al. (2012). In this approach, travel-time residuals are calculated with respect to travel-times predicted by the global ak135 Earth model (Kennett et al., 1995). Prior global body wave tomography studies have shown poor resolution in Antarctica because only about 30 seismic stations across the entire continent report arrivals to the International Seismological Centre (ISC), and most of these stations are located along the coast (Fig. 1). However, in the past few years, several new arrays of autonomous seismographs have been installed in Antarctica (Fig. 1; Suppl. Table 1), providing an important regional dataset with the potential to resolve structural details beneath many parts of the continent. Some notable deployments include the Transantarctic Mountains Seismic Experiment (TAMSEIS), the Transantarctic Mountains Northern Network (TAMNNET), the Gamburtsev Antarctic Mountains Seismic Experiment (GAMSEIS), and the Polar Earth Observing Network (POLENET).

Additionally, we use global travel-time residuals from the re-processed ISC database from Engdahl et al. (1998; EHB database), which includes a wide range of P-wave phases to maximize the effective sampling of the Earth's structure. The EHB catalog used in this study includes over 15 million travel-time residuals associated with more than 496,000 earthquakes, from the time period between January 1964 and October 2007. This dataset contains by far the most arrival times but with a very limited distribution of data for Antarctica (see Suppl. Fig. 2).

The regional Antarctic dataset was manually picked, and travel-time residuals were computed using a slightly modified version of the ak135 reference model, in which appropriate ice and crustal thicknesses were incorporated (Chaput et al., 2014; O'Donnell and Nyblade, 2014). Suppl. Fig. 3 illustrates the consistency of our travel-time residuals both between the EHB catalog and the regional Antarctic data as well as between data from different Antarctic deployments. The total regional network dataset includes over 69,000 travel-time residuals. To balance this smaller but high-quality dataset against the global but somewhat noisier EHB catalog, the regional network data are given twice the weight in the tomographic inversion (Kárason and van der Hilst, 2001; Li et al., 2008).

The combined dataset was inverted for a global model of mantle P-wave structure. Since converging lines of longitude at the Earth's pole cause coordinate singularity difficulties, all station and earthquake locations were rotated prior to inversion such that the new (0°, 0°) origin point is located at the South Pole. Uneven seismic raypath coverage in the mantle can lead to significant lateral variations in resolution; therefore, the tomographic method used here constructs an adaptable grid based on the data sampling density (Kárason and van der Hilst, 2000). One or more cells from a base grid are combined until a minimum ray density in each cell is obtained (Kárason, 2002; Li et al., 2008; Hansen et al., 2012), resulting in an adaptive grid with finer spacing for regions with increased ray coverage (Suppl. Fig. 4). The total number of sampled, adaptive cells used in our inversion is ~500,000. The inversion also takes crustal structure into account through an *a priori* 3D crustal model, which is a modified version of CRUST2.0 (Bassin et al., 2000), with crustal thickness values from Chaput et al. (2014) and O'Donnell and Nyblade (2014) substituted into the region covering the Antarctic continent. This approach balances the crust and upper mantle contributions to the misfit (Li et al., 2008).

The sensitivity matrix calculations are fully described by Kárason (2002) and Li et al. (2008). Briefly, short-period data are back-projected along raypaths calculated in the reference model,

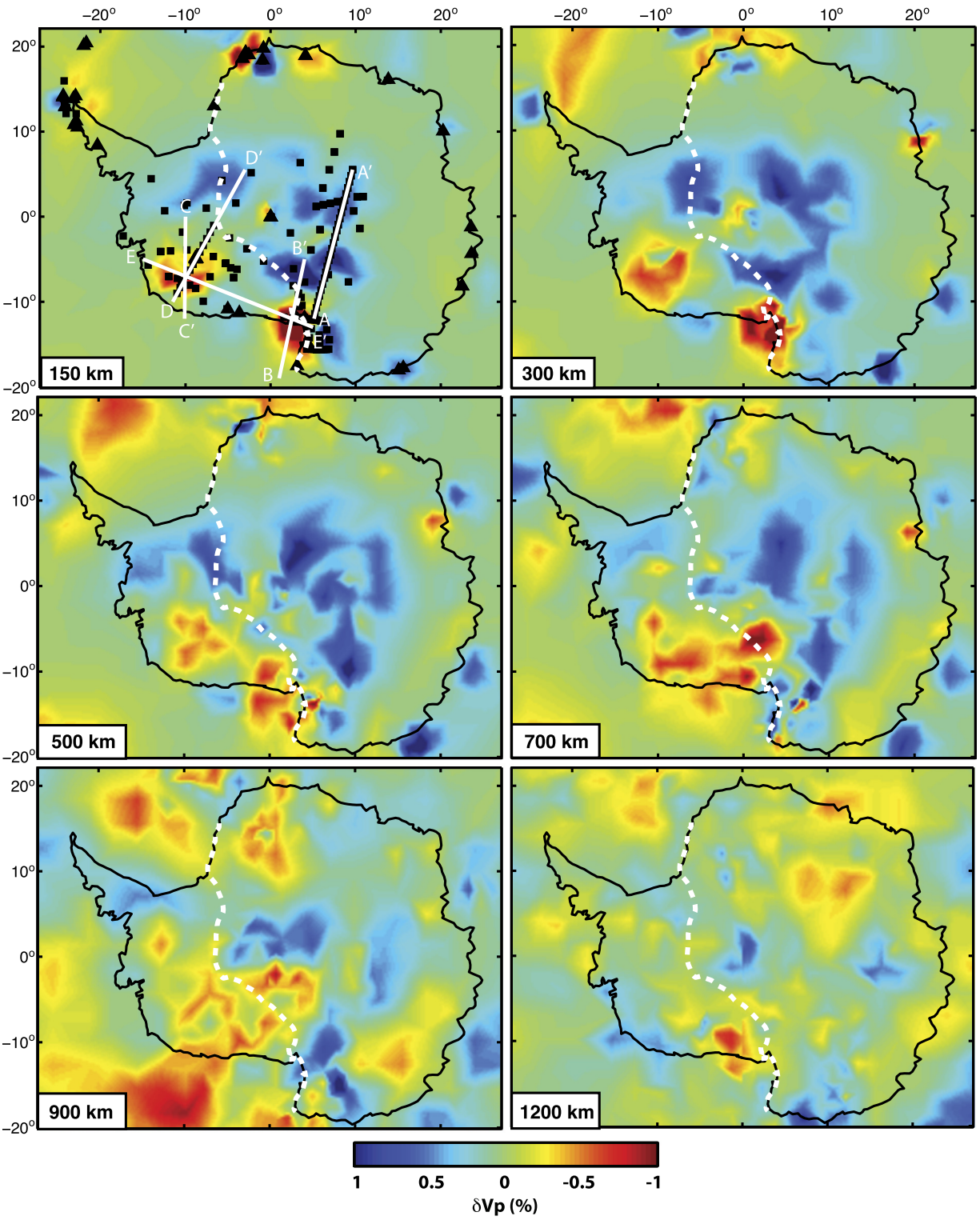

Fig. 2. P-wave tomography image. P-wave velocity perturbations (δV_P) are shown at selected mantle depths. The white dashed line on each panel marks the boundary between East and West Antarctica (Fig. 1). The locations of cross-sectional profiles (Figs. 3–5, 7) are shown in the first panel. The first panel also shows the locations of stations used in this study, where black triangles denote EHB stations and black squares denote Antarctic regional network stations. All panels here, and in subsequent figures, are plotted in the rotated Grid North coordinate system used for the inversion, where latitude and longitude are relative to South Pole.

and weighted composite rays are used to reduce the size of the sensitivity matrix (Spakman and Nolet, 1988; Kárason and van der Hilst, 2001). For long-period data, 3D sensitivity kernels are approximated following Kárason and van der Hilst (2001). This approach allows the long wavelength structure to be constrained by the low-frequency data without preventing short-period data from resolving smaller scale structure.

4. Results and resolution tests

The P-wave velocity perturbations (δV_P) in our model (Fig. 2) were obtained after 200 iterations of the inversion and correspond to a 92% reduction of the objective function. The associated residual vector decreased from 0.96 to 0.29 s. Our model displays considerably more mantle heterogeneity beneath Antarctica com-

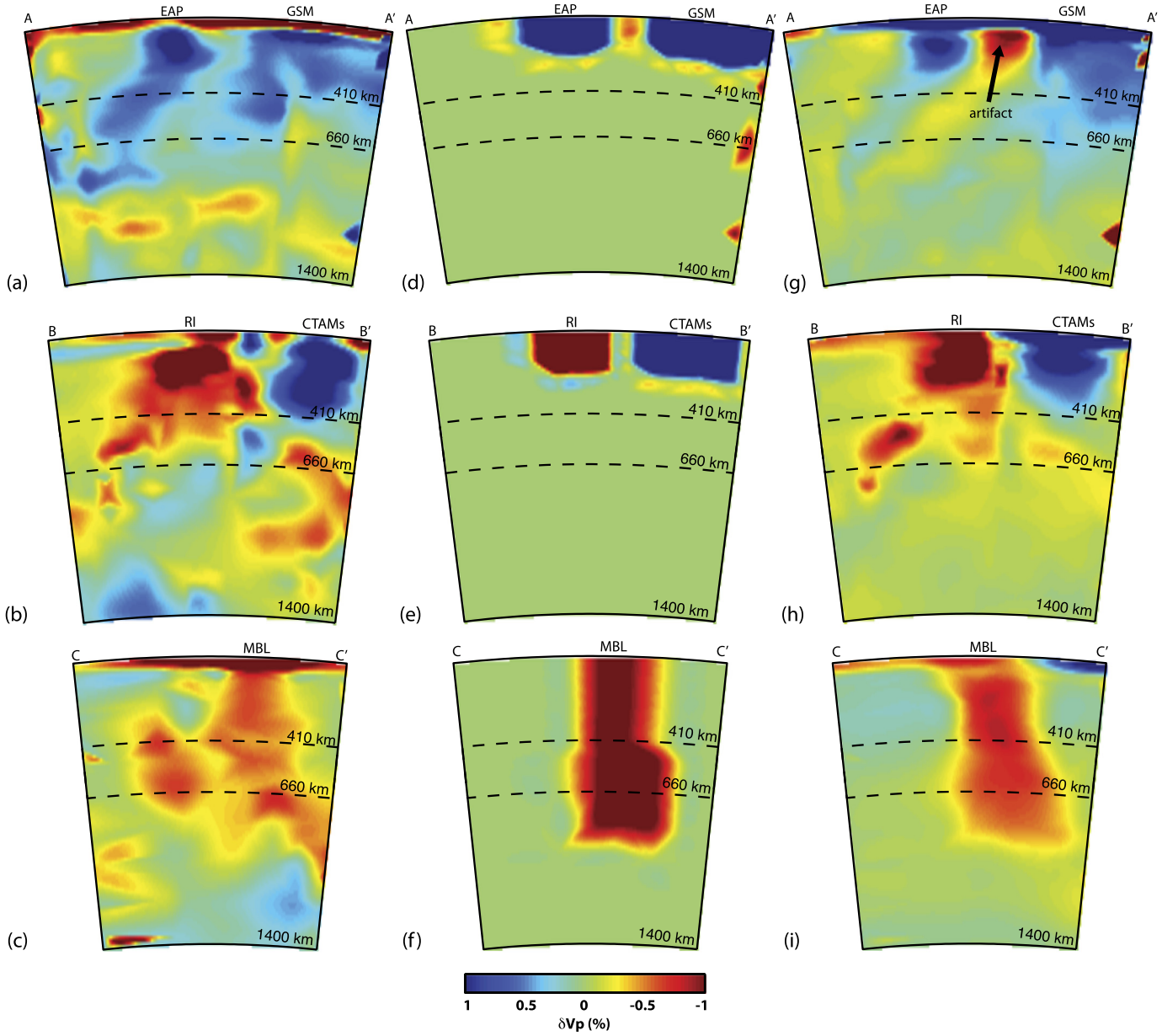

Fig. 3. (a–c) Cross-sections through the tomographic model along profiles A–A′, B–B′, and C–C′. The locations of the cross-sectional profiles are shown in Fig. 2. (d–f) Synthetic tests to examine the extent of vertical smearing in our model. These input models best approximate major features of the observed structure shown in panels (a–c). The input anomalies have been projected onto the adaptive grid (Suppl. Fig. 4). (g–i) Recovered synthetic models. All panels are plotted with a ±1% color scale for direct comparison. Also, the dashed lines in each panel mark the 410 and 660 km discontinuities. Abbreviations for geographic locations are the same as in Fig. 1, except for CTAMs: central TAMs, EAP: East Antarctica Plateau. (For interpretation of the references to color in this figure, the reader is referred to the web version of this article.)

pared to previously developed continental-scale models (*e.g.* Roult and Rouland, 1994; Ritzwoller et al., 2001; Sieminski et al., 2003; Morelli and Danesi, 2004). For instance, fast velocities expected beneath East Antarctica are observed, but fast velocities are also seen beneath the EWM in West Antarctica. Slow velocities are seen beneath both MBL and RI in West Antarctica, but the amplitudes of these anomalies are quite different from one another and do not extend across all of West Antarctica, as in most previously published continental-scale models.

Cross-sections through the model (Figs. 3a–c, 4a, 5a) also highlight the variable structure across Antarctica. Fast velocities ($\delta V_P \approx 2\%$) beneath East Antarctica 'smear' to the south–southwest at depth, but appear to be primarily upper mantle features. A 'break' in the fast structure is also observed between the GSM and the TAMs. Pronounced slow velocities ($\delta V_P \approx -2\%$) beneath RI also appear to be primarily concentrated to the upper mantle. This is in contrast to the slow velocities beneath MBL, which extend to greater mantle depths (~1000 km) but which are also associated with a less negative velocity perturbation ($\delta V_P \approx -0.7\%$).

Several tests have been performed to assess model resolution. First, the lateral resolution was examined with a series of checkerboard tests. The input pattern includes 3°-wide anomalies with alternating ±2% velocity variations. Synthetic travel-times were created and inverted using the same model parameterization as was used for the data, and noise was added to the synthetic travel-times as a Gaussian residual time error with a standard deviation of 0.29 s, which corresponds to the residual remaining in our model after inversion. Given the uneven station distribution, the resolution of our model varies spatially, but the checkerboard pattern is well recovered across western and central–eastern Antarctica, coinciding with the included station locations (Fig. 6). Our best amplitude recovery is ~40–60% due, in a large part, to

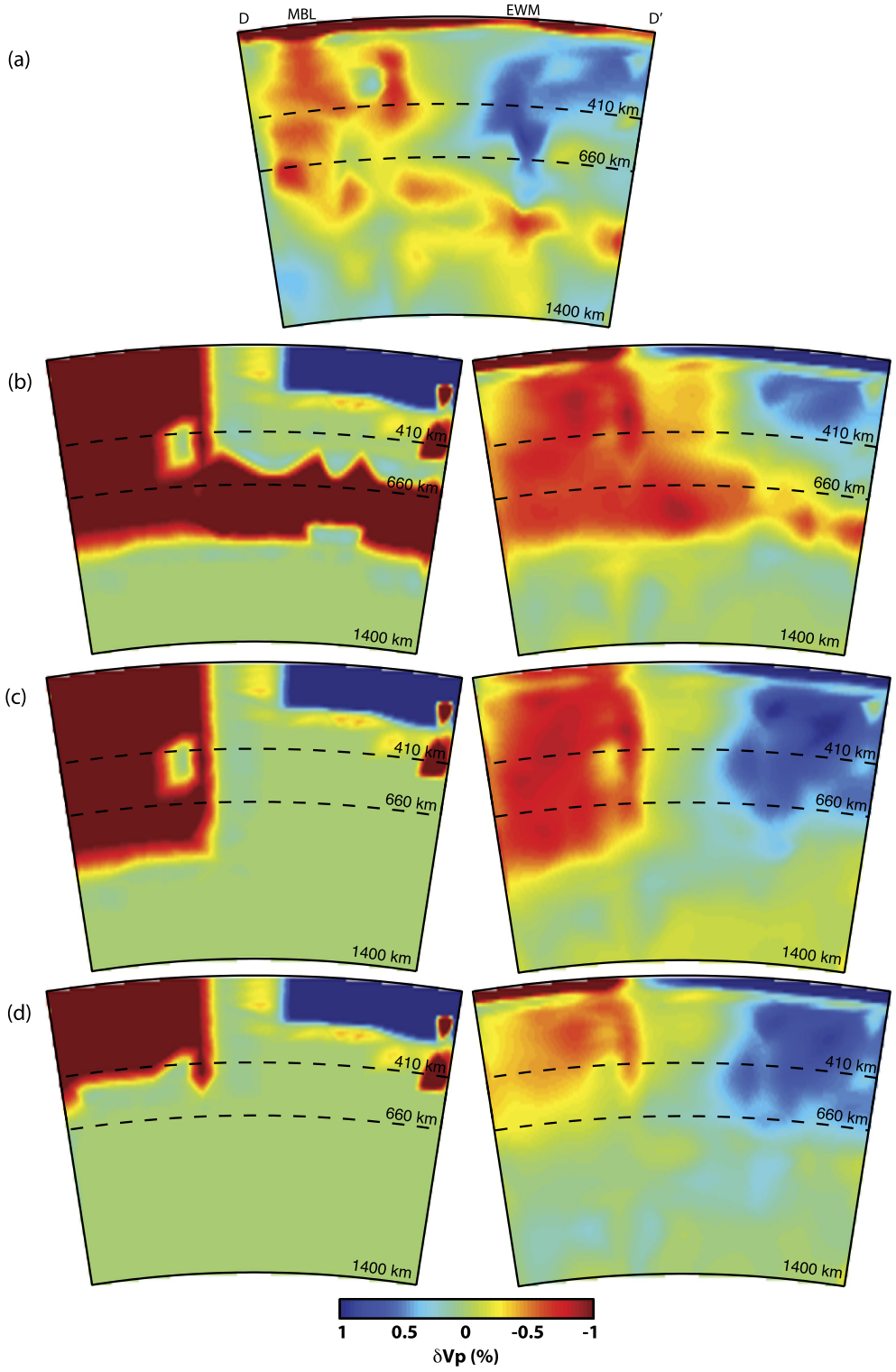

Fig. 4. (a) Cross-section along profile D–D′ (Fig. 2). (b–d) Synthetic tests along profile D–D′. Input models are shown on the left and recovered models are shown on the right. The input anomalies have been projected onto the adaptive grid (Suppl. Fig. 4). (b) The synthetic model that best matches the observed structure, with a ∼800 km deep, −1% anomaly beneath MBL, a ∼200 km thick, 4% anomaly beneath the EWM, and slow (−2%) velocities extending laterally below the transition zone. (c) Same as model (b) but without the slow anomaly below the transition zone. (d) Same as model (c) but with a shallower (∼400 km) anomaly beneath MBL. Abbreviations for geographic locations are the same as in previous figures, and all panels have been plotted with the same color scale for direct comparison.

regularization parameters used to stabilize the solution of the inversion.

The vertical resolution of our model was assessed with synthetic anomalies that match major observed features (Fig. 3d–i). Along profiles A–A′ and B–B′, fast synthetic anomalies are used to match the structure beneath East Antarctica, the TAMs, and the GSM, while a slow synthetic anomaly is used to match the structure beneath RI (Fig. 3d–e). The thickness of each of these anomalies is ∼200 km. Since the amplitude recovery of our model is ∼40–60%, as indicated by the checkerboard resolution tests (Fig. 6), we have roughly doubled the observed velocity perturbations, giving the East Antarctic and RI synthetic anomalies input amplitudes

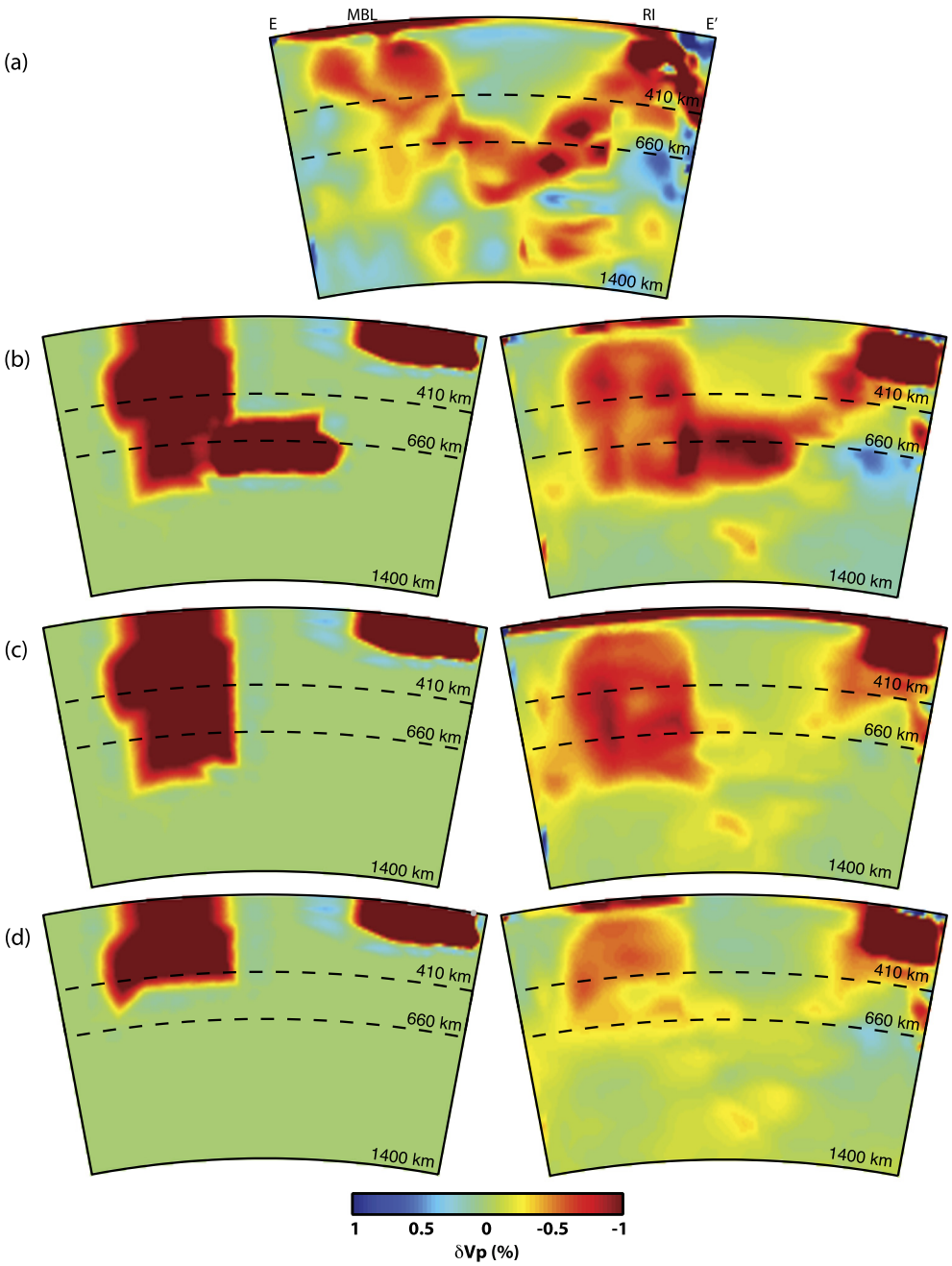

Fig. 5. (a) Cross-section along profile E–E′ (Fig. 2). (b–d) Synthetic tests along profile E–E′. Input models are shown on the left and recovered models are shown on the right. The input anomalies have been projected onto the adaptive grid (Suppl. Fig. 4). (b) The synthetic model that best matches the observed structure, with a ∼200 km thick, −4% anomaly beneath RI, a ∼800 km thick, −1% anomaly beneath MBL, and slow (−2%) velocities extending laterally below the transition zone below West Antarctica, similar to Fig. 4. (c) Same as model (b) but without the slow anomaly below the transition zone. (d) Same as model (c) but with a shallower (∼400 km) anomaly beneath MBL. Abbreviations for geographic locations are the same as in previous figures, and all panels have been plotted with the same color scale for direct comparison.

that are 4% faster and slower than the reference model, respectively. The recovered images (Fig. 3g–h) show ∼200 km of vertical smearing. This is not atypical for P-wave tomography studies. Smearing is more pronounced in the south–southwest direction, similar to our model. Along profile A–A′, the abrupt change between adjacent grid cells results in an artificial slow anomaly between the fast regions of the input model, and this shows up as an artifact in the recovered model, but the fast synthetic structure matches the observed structure (Fig. 3a) fairly well. A synthetic anomaly associated with the slow velocities beneath MBL (profile C–C′, Fig. 3f) is also examined. In this case, an input amplitude of −1% is used, and the synthetic anomaly extends to ∼800 km depth (Fig. 3f). The level of vertical smearing is somewhat less extensive in the recovered image (∼100–150 km; Fig. 3i), likely due to the better resolution in our model at mid-mantle depths (Fig. 6; Suppl. Fig. 4).

A series of squeeze tests (*e.g.*, Schutt and Humphreys, 2004; Allen and Tromp, 2005) were also used to assess the vertical resolution of our velocity model. Squeezing was implemented through a two-stage inversion. During the first-stage, damping parameters were specified such that the velocity anomalies were only permitted within a specified depth range. The residual data vector (i.e. the projection of the travel-time data that cannot be satisfied by anomalies within the allowed depth range) were then input into a second stage of the inversion, where the anomalies are allowed throughout the whole model space. If the residuals from the first

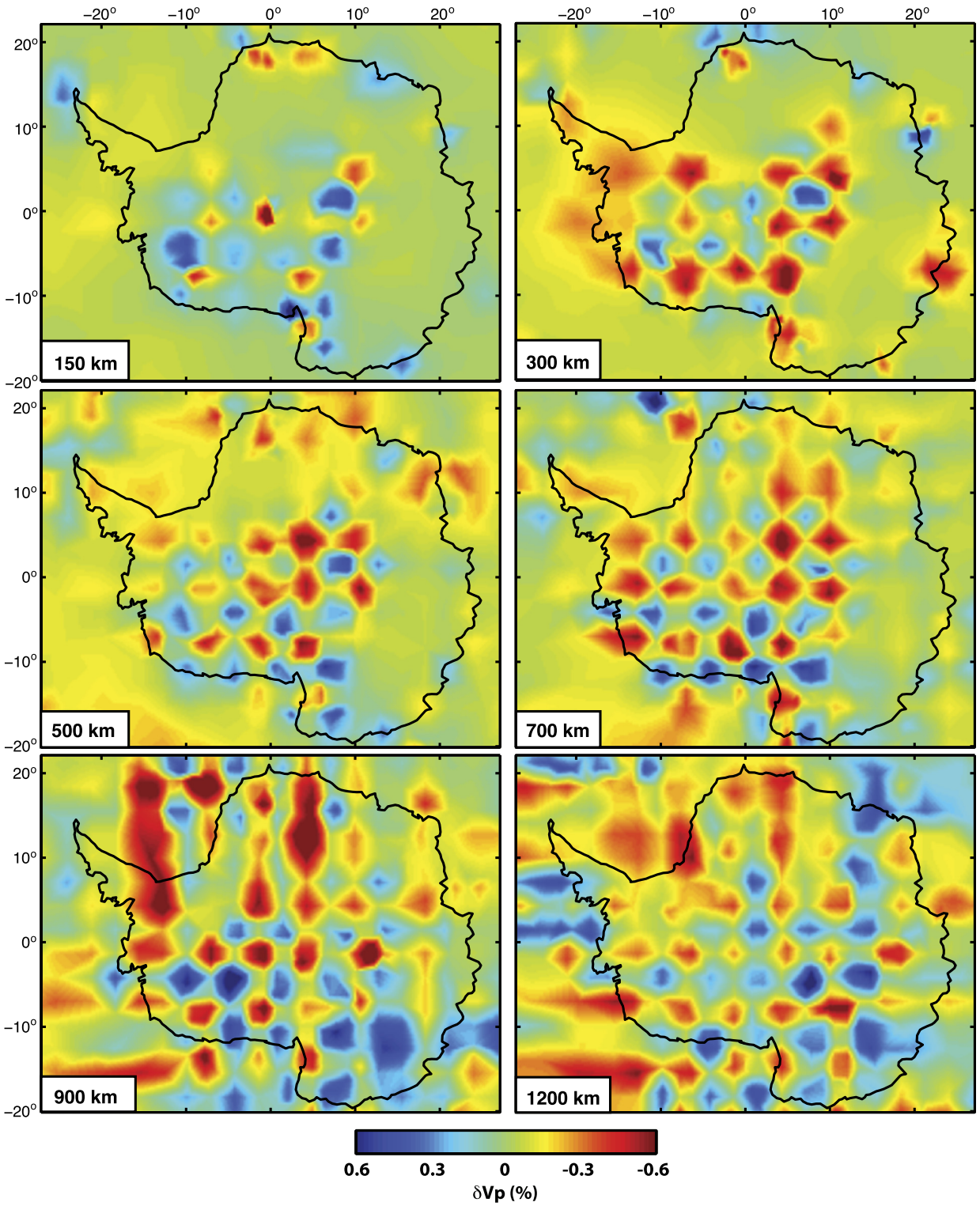

Fig. 6. Results from checkerboard resolution tests, show at selected mantle depths. All images have been plotted with the same color scale so that the degree of pattern and amplitude recovery can be easily compared. The input pattern consists of 3°-wide anomalies with alternating ±2% velocity variations.

stage of the inversion are small, indicating that the squeezed structure is adequate to fit the data, then no significant new structure will be generated in the second stage. Otherwise, if structure outside the initially specified depth range is required to fit the data, significant anomalies outside of the initial constrained depths will be generated.

The vertical extent of the mantle anomalies in our tomographic model were tested using squeezing depths ranging from 200–1000 km, which constrained the velocity perturbations to shallower portions of the model space (Fig. 7). The depth constraints provided by the squeeze tests are similar to those indicated by our synthetic resolution tests. For example, the slow anomaly beneath MBL appears to extend to ∼1000 km depth in our model (Fig. 3c), but the squeeze test results indicate this feature could be constrained to depths ∼800–850 km (i.e. ∼150–200 km shallower but still extending to the mid-mantle).

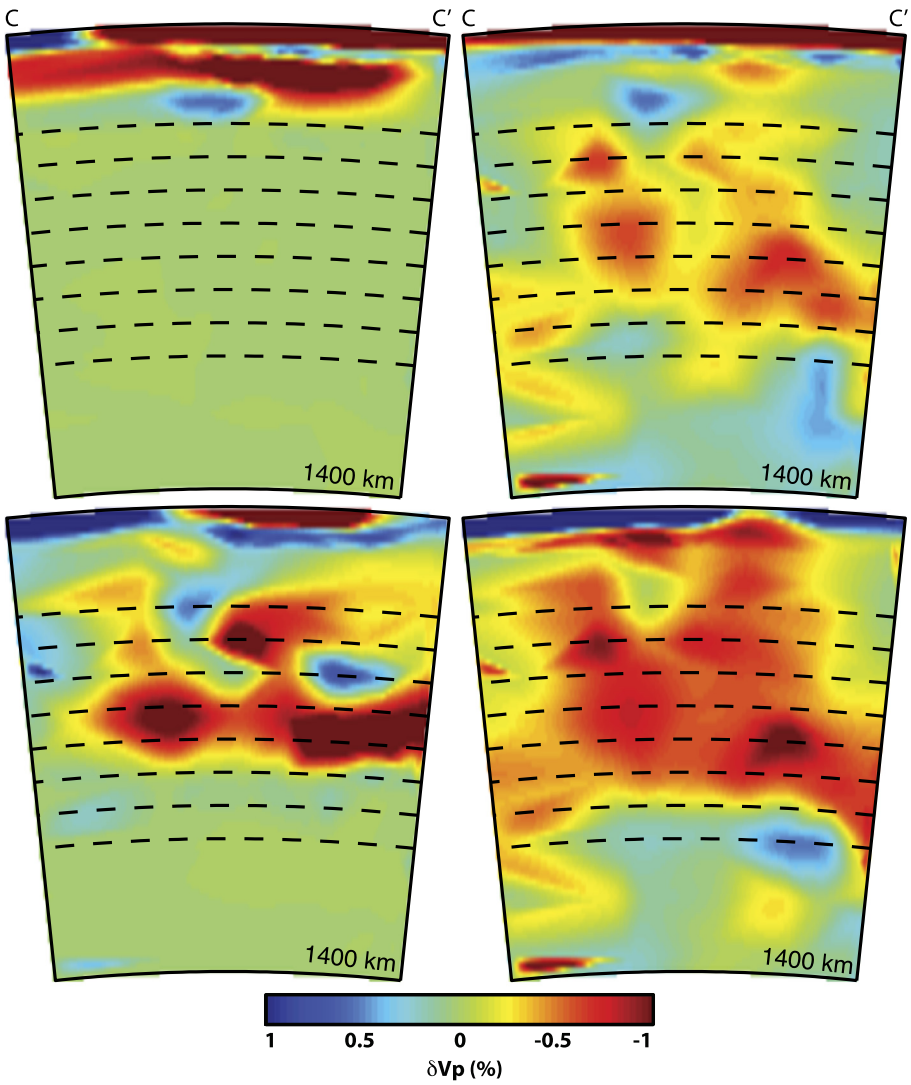

Fig. 7. Examples of squeeze tests, examining the mantle structure along profile C–C′ (Fig. 2). Dashed lines mark depths of 300–1000 km in 100 km increments. The models on the left have been squeezed to (top) 300 km and (bottom) 800 km, respectively. The models on the right are the corresponding results of the full, two-stage squeezed inversion. Note that when the model is not over-squeezed (as in the 300 km case), the low-velocity structure does retreat to somewhat shallower depths.

5. Discussion

Our adaptively parameterized model reveals considerable mantle heterogeneity, with a range of velocity variations, particularly beneath parts of the TAMs and West Antarctica. Constraints on this type of mantle heterogeneity are important for tectonic interpretations as well as for glacial isostatic adjustment modeling. The two most significant features in our model are the slow velocity anomalies beneath RI and MBL, and the following subsections discuss these features in further detail.

5.1. TAMs and the Ross Island anomaly

Previous continental-scale seismic models for Antarctica indicate that the TAMs overlie a boundary between fast mantle in East Antarctica and slow mantle in West Antarctica (*e.g.* Roult and Rouland, 1994; Ritzwoller et al., 2001; Sieminski et al., 2003; Morelli and Danesi, 2004). Regional studies (Watson et al., 2006; Lawrence et al., 2006a) suggest that in the vicinity of RI, the transition from fast to slow velocities occurs about 50–100 km inland from the coast. However, these regional models lose resolution away from RI, so the lateral extent of the slow velocities is not well constrained. Heeszel (2011) suggested the slow velocities extend across the WARS, adjacent to the TAMs at upper mantle depths ($<\sim$200 km), but did not provide constraints on the extent of the slow velocities toward grid south.

The addition of TAMNNET (not used in any previous tomographic studies) and other recent data allows us to further assess the structure beneath the TAMs and RI region. In our model, a sharp contrast is observed between the fast velocities of the central TAMs and the slow velocities beneath RI (Figs. 2, 3b), with the boundary $\sim$100–150 km inland from the coast, similar to Watson et al. (2006) and Lawrence et al. (2006a). However, our model shows that the RI slow anomaly extends grid south towards Victoria Land (Fig. 2), with the fast-to-slow boundary continuing beneath the TAMs front. The lateral extent of this slow anomaly has important implications in terms of uplift models for the TAMs. Flexural uplift models (Stern and ten Brink, 1989; ten Brink et al., 1997) invoke a thermal buoyancy load in the upper mantle, and the slow velocity anomaly extending beneath the TAMs front beneath RI and Victoria Land is consistent with a thermally perturbed lithosphere. Therefore, we support a thermal contribution to the uplift for this portion of the TAMs. However, our model does not indicate that the RI anomaly extends grid north along the TAMs and into the WARS at mantle depths $\geq\sim$200 km.

Therefore, upper mantle thermal contributions to the TAMs uplift likely vary along strike.

Some studies favor a plume source to explain the slow seismic velocities and volcanism associated with RI (*e.g.*, Behrendt et al., 1991). For instance, Kyle et al. (1992) and Esser et al. (2004) explored a plume model, with a 40 km diameter plume head, to explain petrologic observations. Our model indicates that the RI anomaly is constrained to the upper ~200–300 km of the mantle, consistent with Reusch et al. (2008), so there is little evidence for a lower mantle upwelling beneath this region. Additionally, the lateral extent of the RI slow anomaly from our model (Fig. 2) indicates that the plume head diameter, if present, would need to be much larger than that suggested by Kyle et al. (1992) and Esser et al. (2004). Our findings agree well with Cooper et al. (2007), who geochemically linked volcanic deposits separated by over 140 km throughout the Ross Sea region. This and other studies (*e.g.*, Rocchi et al., 2002, 2003, 2005) instead suggest that the volcanism and slow seismic velocities in this area are better explained by locally focused rift-related decompression melting and shallow convection. The amplitude of the RI low velocity anomaly in our model is very pronounced (~−4% indicated by the synthetic tests), and we interpret this feature as the signature of Cenozoic extension beneath Terror Rift (Wannamaker et al., 1996; Karner et al., 2005).

5.2. West Antarctica and the Marie Byrd Land anomaly

In West Antarctica, our model shows fast seismic velocities beneath parts of the EWM and slow velocities beneath MBL (Figs. 2, 4a). This structure is more heterogeneous than those shown in previous continental-scale models for Antarctica (*e.g.*, Roult and Rouland, 1994; Ritzwoller et al., 2001; Sieminski et al., 2003; Morelli and Danesi, 2004), but they agree well with regional seismic models developed using the POLENET dataset. For example, Heeszel (2011) and Lloyd et al. (2013b) both show that the EWM are underlain by seismic velocities that are fast relative to the rest of West Antarctica, extending to ~150–250 km in the mantle, while MBL is underlain by slow seismic velocities down to at least ~300–400 km depth. However, the resolution of these regional models at depths greater than ~300–400 km markedly decreases, making it difficult to assess if the MBL low velocity anomaly extends into or deeper than the transition zone. An earlier study by Sieminski et al. (2003) indicated that deep-seated low velocities beneath West Antarctica were possible. Resolving the velocity structure at mid-mantle depths is critical to assess the geodynamics beneath West Antarctica.

All three cross-sectional profiles that transect MBL in our model (Figs. 2, 3c, 4a, 5a) show that the slow velocities extend through the transition zone. Additionally, profile D–D′ (Fig. 4a) illustrates that the slow velocities extend laterally beneath the EWM. From profile E–E′ (Fig. 5a), it appears that the MBL slow anomaly may potentially connect with the slow anomaly seen beneath RI at deep mantle depths. To assess the resolution of the MBL low velocity structure, additional synthetic tests were performed. These tests indicate that the MBL slow anomaly extends to ~800 km depth (Figs. 3i, 4b, and 5b). The relatively low δV_P of this feature is best matched using an input amplitude of −1% for the corresponding synthetic anomaly. Shallower synthetic anomalies with greater perturbations (i.e. −2%) were also tested, but the corresponding recovered amplitudes did not match our observations well, and while these anomalies do smear to somewhat deeper depths in the mantle, they still did not match the observed depth extent of the MBL feature in our model (Suppl. Fig. 5).

Additionally, to match the structure seen along profiles D–D′ and E–E′ (Figs. 4a, 5a), the slow velocities were extended laterally at depth (Figs. 4b, 5b), with the slow anomaly extending below the transition zone beneath the EWM (Fig. 4b). Synthetic tests illustrate that a somewhat more negative (−2%) input amplitude for the anomalies at these depths with a thickness of ~100–200 km matches the observed structure well. Again, shallower slow anomalies and those without the lateral extension at depth do not match our observations (Fig. 4c–d).

A similar synthetic structure can also explain the observations along profile E–E′ (Fig. 5b). Again, the synthetic anomaly beneath MBL extends to ~800 km depth while the anomaly beneath RI only extends to ~200 km depth, similar to the synthetic test shown in Fig. 3e. The corresponding amplitudes of these two anomalies are quite different, with the RI anomaly being more pronounced. If the slow velocities beneath MBL are allowed to extend laterally below the transition zone, as in the synthetic tests along profile D–D′, the recovered model matches our observed image well (Fig. 5b). These results illustrate that the MBL and RI anomalies are distinct mantle features and only appear to be connected at depth due to smearing in the model. Additionally, the MBL anomaly requires an appreciable lateral extent beneath the transition zone to best match the observed structure (Fig. 5b–d).

Numerous studies have attributed the topographic doming of MBL as well as the composition and spatial distribution of volcanic rocks in this area to a plume-related origin (*e.g.* Behrendt et al., 1991; Hole and LeMasurier, 1994; Weaver et al., 1994; Hart et al., 1997; LeMasurier, 2008). Narrow plume tails are notoriously difficult to image; however, if plume head material were ponded in the upper mantle, the thickness of low velocity material is expected to be ~100–200 km (Ebinger and Sleep, 1998; Davaille et al., 2005; Montelli et al., 2006; Hwang et al., 2011), which is much thinner than the low velocity anomaly imaged in our model. However, our tomographic model and associated synthetic tests indicate that slow velocities extend laterally below the transition zone beneath West Antarctica. We suggest that if a plume is present beneath this area, then the plume head has ponded below the transition zone.

Numerous geodynamic and seismic studies have suggested that the 660 km endothermic phase boundary may present an obstacle for plumes ascending through the lower mantle, which would cause the plume to spread beneath the transition zone (*e.g.*, Davies, 1995; Vinnik et al., 1997; Cserepes and Yuen, 2000; Farnetani and Hofmann, 2009). The thickness of the deep anomaly indicated by our model and synthetic tests is consistent with that expected for ponded plume head material (~100–200 km; Ebinger and Sleep, 1998; Davaille et al., 2005; Montelli et al., 2006) and such a feature would thermally perturb the overlying mantle, leading to the low velocities seen throughout the mantle beneath MBL. Thermal buoyancy from this deep, anomalous structure would also help provide uplift for the EWM.

A recent receiver function study (Emry et al., submitted for publication) indicates that the 410 km seismic discontinuity is depressed beneath all of West Antarctica, consistent with a broad region of low velocities in the overlying mantle. The mantle transition zone thickness is fairly consistent with the global average; however, notable exceptions are observed beneath the MBL Ruppert Coast and below the EWM and Bentley Subglacial Trench, where the transition zone is thinned. Emry et al. (submitted for publication) suggest that the mantle transition zone beneath West Antarctica may be hotter than average in these two locations, caused by thermal upwellings from the lower mantle. A plume head ponded below the transition zone, as suggested above, would provide a source of heat for the overlying mantle and could lead to secondary upwellings, consistent with Emry et al. (submitted for publication).

5.3. East Antarctica

Most of East Antarctica is underlain by fast seismic velocities in our model, consistent with previous continental-scale studies (Figs. 2, 3a–b; *e.g.*, Roult and Rouland, 1994; Ritzwoller et al., 2001; Morelli and Danesi, 2004). Taking the amount of vertical smearing indicated by our synthetic and squeeze tests into account (Figs. 3g–h, 7), the fast velocities beneath East Antarctica extend to ~200–250 km depth. This estimate also agrees well with regional seismic investigations (Lawrence et al., 2006a; Heeszel et al., 2013; Lloyd et al., 2013a), which support the conclusion that East Antarctica is underlain by thick Archean or Proterozoic cratonic lithosphere. Somewhat slower mantle velocities are observed near the PSB (Figs. 2, 3a), also consistent with prior regional seismic studies (Hansen et al., 2010; Heeszel et al., 2013; Lloyd et al., 2013a). It has been shown that this area is also associated with a significant aeromagnetic anomaly, and it has been suggested that the distinct geophysical features here relate to a ~1.1–1.9 Ga period of orogenic activity (Finn et al., 2006; Goodge et al., 2008; Goodge and Finn, 2010).

6. Conclusions

Using an adaptively parameterized tomography method, integrating travel-time data from a number of recent deployments, we have developed the first continental-scale image of P-wave speed variations for the Antarctic mantle. Our model resolves considerably more heterogeneity across the continent, particularly in West Antarctica, than previously developed continental-scale models and provides higher resolution imaging of deeper mantle structure than that provided by regional-scale models. These attributes are important to assess the geodynamic processes shaping the Antarctic continent.

Our model places lateral constraints on the slow velocity anomaly beneath RI. This anomaly extends towards Victoria Land, further grid south than has been recognized in previous studies. The boundary between these slow velocities and the fast velocities underlying East Antarctica is found ~100–150 km beneath the TAMs front, supporting flexural uplift models (Stern and ten Brink, 1989; ten Brink et al., 1997) for this portion of the TAMs. However, at least at mantle depths $\geq$~200 km, the slow anomaly does not extend grid north along the TAMs and into the WARS. The lateral extent of these low velocities is best explained by rift-related decompression melting and shallow convection (Wannamaker et al., 1996; Karner et al., 2005; Cooper et al., 2007; Rocchi et al., 2002, 2003, 2005).

In West Antarctica, MBL is underlain by a deep-seated (~800 km) low velocity anomaly with a relatively low δV_P signature. Synthetic tests illustrate that the low velocities extend laterally below the transition zone, and this structure has been interpreted as a mantle plume ponded below the 660 km discontinuity, which would thermally perturb the overlying mantle. The slow anomalies beneath MBL and RI are separate features from one another and highlight the variable structure across West Antarctica.

Acknowledgements

We thank R. van der Hilst and S. Burdick for providing the tomography software and the Incorporated Research Institutions for Seismology (IRIS) Data Management System for data handling assistance. We also thank two anonymous reviewers for their thorough critiques of this manuscript. The facilities of the IRIS Consortium are supported by the National Science Foundation (NSF) under cooperative agreement EAR-1063471, the NSF Office of Polar Programs, and the Department of Energy National Nuclear Security Administration. Funding for this research was provided by the NSF (grant numbers PLR-0851560, ANT-1139739, PLR-1141916, PLR-0632230, PRL-0632239, PLR-0652322, PLR-0632335, PLR-0632136, PLR-0632209, PLR-0632185, and PLR-1246712).

Appendix A. Supplementary material

Supplementary material related to this article can be found online at http://dx.doi.org/10.1016/j.epsl.2014.09.043.

References

Allen, R.M., Tromp, J., 2005. Resolution of regional seismic models: squeezing the Iceland anomaly. Geophys. J. Int. 161, 373–386.
Anthony, R., Aster, R., Wiens, D., Nyblade, A., Anandakrishnan, S., Winberry, J.P., Wilson, T., Rowe, C., submitted for publication. The seismic noise environment of Antarctica. Seismol. Res. Lett.
Barrett, P.J., Hambrey, M.J., Harwood, D.M., Pyne, A.R., Webb, P.N., 1989. Synthesis-Antarctic Cenozoic history from the CIROS-1 drill hole, McMurdo Sound. DSIR Bull. 245, 241–251.
Bassin, C., Laske, G., Masters, G., 2000. The current limits of resolution for surface wave tomography in North America. Eos Trans. AGU 81 (48). Fall Meet. Suppl., Abstract S12A-03.
Behrendt, J.C., Cooper, A.K., 1991. Evidence of rapid Cenozoic uplift on the shoulder escarpment of the Cenozoic West Antarctic rift system and a speculation on possible climate forcing. Geology 19, 315–319.
Behrendt, J.C., LeMasurier, W.E., Cooper, A.K., Tessensohn, F., Tréhu, A., Damaske, D., 1991. Geophysical studies of the West Antarctic Rift System. Tectonics 10, 1257–1273.
Behrendt, J.C., Blankenship, D.D., Damaske, D., Cooper, A.K., Finn, C., Bell, R.E., 1997. Geophysical evidence for late Cenozoic subglacial volcanism beneath the West Antarctic Ice Sheet and additional speculation as to its origin. In: The Antarctic Region: Geological Evolution and Processes, pp. 539–546.
Block, A.E., Bell, R.E., Studinger, M., 2009. Antarctic crustal thickness from satellite gravity: implications for the Transantarctic and Gamburtsev Subglacial Mountains. Earth Planet. Sci. Lett. 288, 194–203.
Bott, M.H.P., Stern, H.P., 1992. Finite element analysis of Transantarctic Mountain uplift and coeval subsidence in the Ross Embayment. Tectonophysics 201, 341–356.
Bradshaw, J.D., 1989. Cretaceous geotectonic patterns in the New Zealand region. Tectonics 8, 803–820.
Cande, S.C., Stock, J.M., Muller, R.D., Ishihara, T., 2000. Cenozoic motion between East and West Antarctica. Nature 404, 145–150.
Chaput, J., Aster, R.C., Huerta, A., Sun, X., Lloyd, A., Wiens, D., Nyblade, A., Anandakrishnan, S., Winberry, J.P., Wilson, T., 2014. The crustal thickness of West Antarctica. J. Geophys. Res. 119, 1–18.
Chéry, J., Lucazeau, F., Daignières, M., Vilotte, J.P., 1992. Large uplift of rift flanks: a genetic link with lithospheric rigidity? Earth Planet. Sci. Lett. 112, 195–211.
Clapperton, C.M., Sugden, D.E., 1990. Late Cenozoic glacial history of the Ross Embayment, Antarctica. Quat. Sci. Rev. 9, 253–272.
Clarke, T.S., Burkholder, P.D., Smithson, S.B., Bentley, C.R., 1997. Optimum seismic shooting and recording parameters and a preliminary crustal model for the Byrd Subglacial Basin, Antarctica. In: Ricci, C.A. (Ed.), The Antarctic Region: Geological Evolution and Processes, pp. 485–493.
Cooper, A.F., Adam, L.J., Coulter, R.F., Eby, G.N., McIntosh, W.C., 2007. Geology, geochronology, and geochemistry of a basanitic volcano, White Island, Ross Sea, Antarctica. J. Volcanol. Geotherm. Res. 165, 189–216.
Cserepes, L., Yuen, D.A., 2000. On the possibility of a second kind of mantle plume. Earth Planet. Sci. Lett. 183, 61–71.
Dalziel, I.W.D., 1992. Antarctica: a tale of two supercontinents. Annu. Rev. Earth Planet. Sci. 20, 501–526.
Davaille, A., Stutzmann, E., Silveira, G., Besse, J., Courtillot, V., 2005. Convection patterns under the Indo-Atlantic "box". Earth Planet. Sci. Lett. 239, 233–252.
Davies, G.F., 1995. Penetration of plates and plumes through the mantle transition zone. Earth Planet. Sci. Lett. 133, 507–516.
Ebinger, C.J., Sleep, N.H., 1998. Cenozoic magmatism throughout east Africa resulting from impact of a single plume. Nature 395, 788–791.
Emry, E.L., Nyblade, A., Julia, J., Anandakrishnan, S., Aster, R., Wiens, D., Huerta, A., Wilson, T., submitted for publication. The mantle transition zone beneath West Antarctica: seismic evidence for hydration and thermal upwellings. Geochem. Geophys. Geosyst.
Engdahl, E.R., van der Hilst, R.D., Buland, R., 1998. Global teleseismic earthquake relocation with improved travel times and procedures for depth determination. Bull. Seismol. Soc. Am. 88, 722–743.
Esser, R.P., Kyle, P.R., McIntosh, W.C., 2004. $^{40}Ar/^{39}Ar$ dating of the eruptive history of Mount Erebus, Antarctica: volcano evolution. Bull. Volcanol. 66, 671–686.
Farnetani, C.G., Hofmann, A.W., 2009. Dynamics and internal structure of a lower mantle plume conduit. Earth Planet. Sci. Lett. 282, 314–322.
Ferraccioli, F., Finn, C.A., Jordan, T.A., Bell, R.E., Anderson, L.M., Damaske, D., 2011. East Antarctic rifting triggers uplift of the Gamburtsev Mountains. Nature 479, 388–392.

Finn, C.A., Goodge, J.W., Damaske, D., Fanning, C.M., 2006. Scouting craton's edge in paleo-Pacific Gondwana. In: Antarctica: Contributions to Global Earth Sciences. In: Int. Symp. Ant. Earth Sci., pp. 165–173.
Finotello, M., Nyblade, A., Julià, J., Wiens, D., Anandakrishnan, S., 2011. Crustal V_p–V_s ratios and thickness for Ross Island and the Transantarctic Mountain front, Antarctica. Geophys. J. Int. 185, 85–92.
Fitzgerald, P.G., 1992. The Transantarctic Mountains of southern Victoria Land: the application of apatite fission track analysis to a rift shoulder uplift. Tectonics 11, 634–662.
Fitzgerald, P.G., 1994. Thermochronologic constraints on post-Paleozoic tectonic evolution of the central Transantarctic Mountains, Antarctica. Tectonics 13, 818–836.
Fitzgerald, P., Baldwin, S., 1997. Detachment fault model for the evolution of the Ross Embayment. In: Ricci, C.A. (Ed.), The Antarctic Region: Geological Evolution and Processes, pp. 555–564.
Fitzgerald, P.G., Sandiford, M., Barrett, P.J., Gleadow, A.J.W., 1986. Asymmetric extension associated with uplift and subsidence in the Transantarctic Mountains and Ross Embayment. Earth Planet. Sci. Lett. 81, 67–78.
Fitzsimons, C.W., 2000. Grenville-age basement provinces in East Antarctica: evidence for three separate collisional orogens. Geology 28, 879–882.
Fitzsimons, C.W., 2003. Proterozoic basement provinces of southern and southwestern Australia, and their correlation with Antarctica. Geol. Soc. (Lond.) Spec. Publ. 206, 93–130.
Fretwell, P., et al., 2013. BEDMAP2: improved ice bed, surface and thickness datasets for Antarctica. Cryosphere 7, 375–393.
Goodge, J.W., Finn, C.A., 2010. Glimpses of East Antarctica: aeromagnetic and satellite magnetic view from the central Transantarctic Mountains of East Antarctica. J. Geophys. Res. 115. http://dx.doi.org/10.1029/2009JB006890.
Goodge, J.W., Fanning, C.M., Bennett, V.C., 2001. U–Pb evidence of approximately 1.7 Ga crustal tectonism during the Nimrod Orogeny in the Transantarctic Mountains, Antarctica: implications for Proterozoic plate reconstructions. Precambrian Res. 112, 261–288.
Goodge, J.W., Vervoort, J.D., Fanning, C.M., Brecke, D.M., Farmer, G.L., Williams, I.S., Myrow, P.M., DePaolo, D.J., 2008. A positive test of East Antarctica–Laurentia juxtaposition within the Rodinia supercontinent. Science 321, 235–240.
Granot, R., Cande, S.C., Stock, J.M., Davey, F.J., Clayton, R.W., 2010. Postspreading rifting in the Adare Basin, Antarctica: regional tectonic consequences. Geochem. Geophys. Geosyst. 11. http://dx.doi.org/10.1029/2010GC003105.
Groushinsky, N.P., Sazhina, N.B., 1982. Gravitational field of Antarctica. Int. Union Geol. Sci. 4, 913–917.
Hansen, S.E., Julià, J., Nyblade, A.A., Pyle, M.L., Wiens, D.A., Anandakrishnan, S., 2009. Using S wave receiver functions to estimate crustal structure beneath ice sheets: an application to the Transantarctic Mountains and East Antarctic craton. Geochem. Geophys. Geosyst. 10. http://dx.doi.org/10.1029/2009GC002576.
Hansen, S.E., Nyblade, A.A., Heeszel, D.S., Wiens, D.A., Shore, P., Kanao, M., 2010. Crustal structure of the Gamburtsev Mountains, East Antarctica, from S-wave receiver functions and Rayleigh wave phase velocities. Earth Planet. Sci. Lett. 300, 395–401.
Hansen, S.E., Nyblade, A.A., Benoit, M.H., 2012. Mantle structure beneath Africa and Arabia from adaptively parameterized P-wave tomography: implications for the origin of Cenozoic Afro-Arabian tectonism. Earth Planet. Sci. Lett. 319–320, 23–34.
Hart, S.R., Blusztajn, J., LeMasurier, W.E., Rex, D.C., 1997. Hobbs Coast Cenozoic volcanism: implications for the West Antarctic rift system. Chem. Geol. 139, 223–248.
Heeszel, D.S., 2011. Surface wave derived shear velocity structure of the Gamburtsev Subglacial Mountains, Transantarctic Mountains, and West Antarctica and shallow seismicity of the Mariana and Tonga Subduction Zones. PhD Dissertation. Washington University in St. Louis.
Heeszel, D.S., Wiens, D.A., Nyblade, A.A., Hansen, S.E., Kanao, M., An, M., Zhao, Y., 2013. Rayleigh wave constraints on the structure and tectonic history of the Gamburtsev Subglacial Mountains, East Antarctica. J. Geophys. Res. 118, 2138–2153.
Hoffman, S.M., 1991. Petrology and provenance of the Paleocene strata at Cape Wiman, Seymour Island (Antarctic Peninsula). M.S. Thesis. Ohio State University.
Hole, M.J., LeMasurier, W.E., 1994. Tectonic controls on the geochemical composition of Cenozoic, mafic alkaline volcanic rocks from West Antarctica. Contrib. Mineral. Petrol. 117, 187–202.
Hwang, Y.K., Ritsema, J., van Keken, P.E., Goes, S., Styles, E., 2011. Wavefront healing renders deep plumes seismically invisible. Geophys. J. Int. 187, 273–277.
Kárason, H., 2002. Constraints on mantle convection from seismic tomography and flow modeling. Ph.D. Thesis. Massachusetts Institute of Technology.
Kárason, H., van der Hilst, R.D., 2000. Constraints on mantle convection from seismic tomography. In: Richards, M.A., Gordon, R., van der Hilst, R.D. (Eds.), History and Dynamics of Plate Motion. In: Geophys. Monogr. Ser., vol. 121. AGU, Washington, DC, pp. 277–288.
Kárason, H., van der Hilst, R.D., 2001. Tomographic imaging of the lowermost mantle with differential times of refracted and diffracted core phases (PKP, Pdiff). J. Geophys. Res. 106, 6569–6587.
Karner, G.D., Studinger, M., Bell, R.E., 2005. Gravity anomalies of sedimentary basins and their mechanical implications: application to the Ross Sea basins, West Antarctica. Earth Planet. Sci. Lett. 235, 577–596.
Kennett, B.L.N., Engdahl, E.R., Buland, R., 1995. Constraints on seismic velocities in the Earth from travel times. Geophys. J. Int. 122, 108–124.
Kyle, P.R., Moore, J.A., Thirlwall, M.F., 1992. Petrologic evolution of anorthoclase phonolite lavas at Mt. Erebus, Ross Island, Antarctica. J. Petrol. 33, 849–875.
Lawrence, J.F., Wiens, D.A., Nyblade, A.A., Anandakrishnan, S., Shore, P.J., Voigt, D., 2006a. Rayleigh wave phase velocity analysis of the Ross Sea, Transantarctic Mountains, and East Antarctica from a temporary seismograph array. J. Geophys. Res. 111. http://dx.doi.org/10.1029/2005JB003812.
Lawrence, J.F., Wiens, D.A., Nyblade, A.A., Anandakrishnan, S., Shore, P.J., Voigt, D., 2006b. Crust and upper mantle structure of the Transantarctic Mountains and surrounding regions from receiver functions, surface waves, and gravity: implications for uplift models. Geochem. Geophys. Geosyst. 7. http://dx.doi.org/10.1029/2006GC001282.
Lawver, L.A., Royer, J.Y., Sandwell, D.T., Scotese, C.R., 1991. Evolution of the Antarctic continental margin. In: Thomson, M., Crame, J., Thomson, J. (Eds.), Geological Evolution of Antarctica. Cambridge Univ. Press, New York, pp. 533–539.
LeMasurier, W., 2008. Neogene extension and basin deepening in the West Antarctic rift inferred from comparisons with the East African rift and other analogs. Geology 36, 247–250.
Li, C., van der Hilst, R.D., Engdahl, E.R., Burdick, S., 2008. A new global model for 3-D variations of P-wave velocity in the Earth's mantle. Geochem. Geophys. Geosyst. 9. http://dx.doi.org/10.1029/2007GC001806.
Liu, X., Zhao, Y., Liu, X., 2002. Geological aspects of the Grove Mountains, East Antarctica. Bull. R. Soc. N. Z. 35, 161–166.
Lloyd, A.J., Nyblade, A.A., Wiens, D.A., Shore, P.J., Hansen, S.E., Kanao, M., Zhao, D., 2013a. Upper mantle seismic structure beneath central East Antarctica from body wave tomography: implications for the origin of the Gamburtsev Subglacial Mountains. Geochem. Geophys. Geosyst. 14. http://dx.doi.org/10.1002/ggge.20098.
Lloyd, A.J., Wiens, D.A., Nyblade, A., Anandakrishnan, S., Aster, R.C., Huerta, A.D., Wilson, T.J., Shore, P.J., 2013b. Tomographic evidence for recent extension in the Bentley Subglacial Trench and a hotspot beneath Marie Byrd Land. In: AGU 2013 Fall Meet. Abstract T12A-04.
Montelli, R., Nolet, G., Dahlen, F.A., Masters, G., 2006. A catalogue of deep mantle plumes: new results from finite-frequency tomography. Geochem. Geophys. Geosyst. 7. http://dx.doi.org/10.1029/2006GC001248.
Moores, E.M., 1991. Southwest U.S.–East Antarctic (SWEAT) connection: a hypothesis. Geology 19, 425–428.
Morelli, A., Danesi, S., 2004. Seismological imaging of the Antarctic continental lithosphere: a review. Glob. Planet. Change 42, 155–165.
O'Donnell, J.P., Nyblade, A.A., 2014. Antarctica's hypometry and crustal thickness: implications for the origin of anomalous topography in East Antarctica. Earth Planet. Sci. Lett. 388, 143–155.
Reading, A.M., 2006. The seismic structure of Precambrian and early Paleozoic terranes in the Lambert Glacier region, East Antarctica. Earth Planet. Sci. Lett. 244, 44–57.
Reusch, A.M., Nyblade, A.A., Benoit, M.H., Wiens, D.A., Anandakrishnan, S., Voigt, D., Shore, P.J., 2008. Mantle transition zone thickness beneath Ross Island, the Transantarctic Mountains and East Antarctica. Geophys. Res. Lett. 35. http://dx.doi.org/10.1029/2008GL033873.
Ritzwoller, M.H., Shapiro, N.M., Levshin, A.L., Leahy, G.M., 2001. Crustal and upper mantle structure beneath Antarctica and surrounding oceans. J. Geophys. Res. 106, 30645–30670.
Rocchi, S., Armienti, P., D'Orazio, M., Tonarini, S., Wibrans, J.R., Vincenzo, G.D., 2002. Cenozoic magmatism in the western Ross Embayment: role of mantle plume versus plate dynamics in the development of the West Antarctic Rift System. J. Geophys. Res. 107. http://dx.doi.org/10.1029/2001JB000515.
Rocchi, S., Storti, F., Di Vincenzo, G., Rosetti, F., 2003. Intraplate strike-slip tectonics as an alternative to mantle plume activity for the Cenozoic rift magmatism in the Ross Sea region, Antarctica. In: Storti, F., Holdsworth, R.E., Salvini, F. (Eds.), Intraplate Strike-Slip Deformation Belts. Geol. Soc. (Lond.) Spec. Publ. 210, 145–158.
Rocchi, S., Armienti, P., Di Vincenzo, G., 2005. No plume, no rift magmatism in the West Antarctic Rift. In: Foulger, G.R., Natland, J.H., Presnall, D.C., Anderson, D.L. (Eds.), Plates, Plumes, and Paradigms. In: Geol. Soc. Am. Spec. Paper, vol. 388, pp. 435–447.
Rogers, J.J.W., Miller, J.S., Clements, A.S., 1995. A Pan-African zone linking East and West Gondwana. Mem. Geol. Soc. India 34, 11–23.
Roult, G., Rouland, D., 1994. Antarctica I: deep structure investigations inferred from seismology: a review. Phys. Earth Planet. Inter. 84, 15–32.
Schutt, D.L., Humphreys, E.D., 2004. P and S wave velocity and Vp/Vs in the wake of the Yellowstone hot spot. J. Geophys. Res. 109. http://dx.doi.org/10.1029/2003JB002442.
Siddoway, C.S., 2008. Tectonics of the West Antarctic Rift System: new light on the history and dynamics of distributed intracontinental extension. In: Cooper, A.K., Barrett, P.J., Stagg, H., Storey, B., Stump, E., Wise, W., the 10th ISAES Editorial Team (Eds.), Antarctica: A Keystone in a Changing World, Proceedings of the

10th International Symposium on Antarctic Earth Sciences. The National Academic Press, Washington, DC.
Sieminski, A., Debayle, E., Leveque, J.-J., 2003. Seismic evidence for deep low-velocity anomalies in the transition zone beneath West Antarctica. Earth Planet. Sci. Lett. 216, 645–661.
Spakman, W., Nolet, G., 1988. Imaging algorithms, accuracy and resolution in delay time tomography. In: Vlaar, N.J. (Ed.), Mathematical Geophysics: A Survey of Recent Developments in Seismology and Geodynamics, pp. 155–188.
Stern, T.A., ten Brink, U.S., 1989. Flexural uplift of the Transantarctic Mountains. J. Geophys. Res. 94, 10315–10330.
Stock, J., Molnar, P., 1987. Revised history of early Tertiary plate motion in the south–west Pacific. Nature 325, 495–499.
Studinger, M., Bell, R.E., Finn, C.A., Blankenship, D.D., 2002. Mesozoic and Cenozoic extensional tectonics of the West Antarctic Rift system from high-resolution airborne geophysical mapping. Bull. R. Soc. N. Z. 35, 563–569.
Studinger, M., Bell, R.E., Buck, W.R., Karner, G.D., Blankenship, D.D., 2004. Sub-ice geology inland of the Transantarctic Mountains in light of new aerogeophysical data. Earth Planet. Sci. Lett. 220, 391–408.
Sutherland, R., Mortimer, N., Fitzgerald, P., Isaac, M., 2011. Age of formation of the Transantarctic Mountains in relation to reorganization of adjacent oceanic plate boundaries. Int. Symp. Ant. Earth Sci.. Abstract PS11.11.
ten Brink, U.S., Bannister, S., Beaudoin, B.C., Stern, T.A., 1993. Geophysical investigations of the tectonic boundary between East and West Antarctica. Science 261, 45–50.
ten Brink, U.S., Hackney, R.I., Bannister, S., Stern, T.A., Makovsky, Y., 1997. Uplift of the Transantarctic Mountains and the bedrock beneath the East Antarctic ice sheet. J. Geophys. Res. 102, 27603–27621.
Tingey, R.J., 1991. In: Tingey, R.J. (Ed.), The Regional Geology of Archean and Proterozoic Rocks in Antarctica. The Geology of Antarctica. Clarendon Press, Oxford, UK, pp. 1–58.
van der Beek, P., Cloetingh, S., Andriessen, P., 1994. Mechanisms of extensional basin formation and vertical motion of rift flanks: constraints from tectonic modeling and fission track thermochronology. Earth Planet. Sci. Lett. 121, 417–433.
Vinnik, L., Chevrot, S., Montagner, J.P., 1997. Evidence for a stagnant plume in the transition zone? Geophys. Res. Lett. 24, 1007–1010.
von Frese, R.R., Tan, B.L., Kim, J.W., Bently, C.R., 1999. Antarctic crustal modeling from the spectral correlation of free-air gravity anomalies with the terrain. J. Geophys. Res. 104, 25275–25296.
Wannamaker, P.E., Stodt, J.A., Olsen, S.L., 1996. Dormant state of rifting below the Byrd Subglacial Basin, West Antarctica, implied by magnetotelluric (MT) profiling. Geophys. Res. Lett. 23, 2983–2986.
Watson, T., Nyblade, A., Wiens, D.A., Anandakrishnan, S., Benoit, M., Shore, P.J., Voigt, D., VanDecar, J., 2006. P and S velocity structure of the upper mantle beneath the Transantarctic Mountains, East Antarctic craton, and Ross Sea from travel time tomography. Geochem. Geophys. Geosyst. 7. http://dx.doi.org/10.1029/2005GC001238.
Weaver, S.D., Storey, B., Pankhurst, R.J., Mukasa, S.B., Divenere, V.J., Bradshaw, J.D., 1994. Antarctica–New Zealand rifting and Marie Byrd Land lithospheric magmatism linked to ridge subduction and mantle plume activity. Geology 22, 811–814.
Winberry, P.J., Anandakrishnan, S., 2004. Crustal structure of the West Antarctic rift system and Marie Byrd Land hotspot. Geology 32, 977–980.
Yoo, S.C., 1998. Ice sheet effects on receiver functions and crustal structure of West Antarctica. M.S. Thesis. Pennsylvania State University.
Zhao, Y., Song, B., Zhang, Z., Fu, Y., Chen, T., Wang, Y., Ren, L., Yao, Y., Li, J., Liu, X., 1995. Early Paleozoic (Pan African) thermal event of the Larsemann Hills and its neighbours, Prydz Bay, East Antarctica. Sci. Sin. 38, 74–84.